Laboratory Investigation (2012) 92, 1760–1765

Pulmonary imaging with a scanning acoustic microscope discriminates speed-of-sound and shows structural characteristics of disease

Katsutoshi Miura[1] and Seiji Yamamoto[2]

Tissue elasticity can be detected using a scanning acoustic microscope (SAM), whereby acoustic images are created from the speed of sound through tissues. This system discriminated pulmonary tissue components and demonstrated distinct acoustic images of the lung; these results corresponded well to those obtained using the conventional microscope. SAM provides the following benefits: (1) images are acquired in only few minutes without requirement for staining, (2) basic data is obtained for low-frequency ultrasonic examination, and (3) speed of sound from each lesion is digital and comparable among diseases. Comparative analysis of cancer invasion, post-inflammatory fibrosis, and deposition disease was possible using the data obtained with the system, and the results showed good correlation with those using the conventional microscope and by clinical diagnosis. The SAM system is applicable not only to pulmonary diseases but also to various diseases in other organs.

Laboratory Investigation (2012) **92,** 1760–1765; doi:10.1038/labinvest.2012.135; published online 24 September 2012

KEYWORDS: amyloidosis; bronchioloalveolar carcinoma; cancer invasion; emphysema; pulmonary fibrosis; scanning acoustic microscope; tissue elasticity

Ultrasonic examination is a standard procedure for various organs such as the liver, biliary tracts, pancreas, kidney, thyroid, breast, heart, blood vessels, and urogenital organs.

However, it is not used clinically to examine the lung parenchyma, except in ultrasonic endoscopy, because ultrasound is reflected from air–water interfaces.

A scanning acoustic microscope (SAM) is a device that uses ultrasound (frequency, 100 MHz to 3 GHz) to image an object or tissue. As it is known that the harder the tissue, the more the speed of ultrasound,[1] SAM can provide data on the elasticity of cells and tissues.

Although SAM needs thick flat sections in good quality and its usual resolution is actually lower than light microscope, SAM has some advantages such as quick digital imaging without necessity of staining. Since the 1980s, the acoustic properties of many organs and disease states have been investigated using SAM, such as myocardial infarction,[2] gastric carcinoma, kidney,[3] aortic atherosclerosis,[4] and ligaments.[5] To the best of our knowledge, no pulmonary diseases have been reported using SAM yet.

In this report, we explain the usage of SAM to evaluate pulmonary tissue structures using formalin-fixed, paraffin-embedded tissue sections. Although natural acoustic properties of pulmonary tissues were not provided, no significantly variable properties were shown between fresh and fixed tissues. The acoustic images of tissue elements in the lung were produced with 10–15 μm sections using SAM, and the speed of sound through each element under different conditions was assessed with regard to clinical application.

MATERIALS AND METHODS

Materials

Formalin-fixed, paraffin-embedded sections (10–15 μm thick) were used as specimens. Unstained sections were prepared for SAM imaging, and images obtained were compared with the corresponding light microscopic (LM) images. For SAM imaging, a continual section was stained with hematoxylin and eosin, Elastica–Masson, or Congo red.

[1]Departments of Health Science, Pathology and Anatomy, Hamamatsu University School of Medicine, Hamamatsu, Japan and [2]Medical Photonics Research Center, Hamamatsu University School of Medicine, Hamamatsu, Japan
Correspondence: Dr K Miura, MD, PhD, Departments of Health Science, Pathology and Anatomy, Hamamatsu University School of Medicine, 1-20-1 Handa-yama, Higashi-ku, Hamamatsu 431-3192, Japan.
E-mail: kmiura@hama-med.ac.jp

Received 28 March 2012; revised 2 July 2012; accepted 30 July 2012

Tissue Samples

Pulmonary specimens were selected from Hamamatsu University Hospital archives. We examined 10 normal, 10 nonspecific interstitial pneumonias (NSIP), 11 usual interstitial pneumonias (UIP), 18 bronchioloalveolar carcinomas (BACs), 4 adenocarcinomas (ADCs), 2 organizing pneumonias (OPs), 7 pulmonary emphysematous samples from young individuals and 6 from elderly individuals, and 4 amyloid cases.

SAM Observation

For SAM imaging, we used SAM supplied by Honda Electronics, Toyohashi, Japan with a 120-MHz transducer, which has a resolution of approximately 13 μm. SAM functions by directing focused sound from a transducer to a small area of the target object on a glass slide. The sound emitted by an acoustic transducer hits or penetrates the tissue and is reflected onto the surface of the tissue or glass. It is then returned to the detector, which is coincident with the transducer. The speed of sound through the tissue is calculated by comparing the 'time of flight' of the pulse from the surfaces of both tissue and glass.

For SAM imaging, distilled water was applied between the transducer and the section as coupling fluid. After mechanical X–Y scanning, sound speed from each point on the section was calculated and plotted on the screen to create two-dimensional color-coded images. The region of interest (2.4×2.4 mm) for acoustic microscopy was determined from the LM images. Sound speed at 300×300 points was calculated and plotted on the screen to create the images, and sound data from 64 cross points on the lattice screen were used for statistical analysis (Supplementary Material).

Other data such as thickness of the section and attenuation of sound were also available from each point and shown on the screen.

Statistical Analysis

Data of sound speed from each tissue element are given as mean ± standard deviation (s.d.; m/s). Student's *t*-test was used for determining statistical differences among specimens. $P < 0.01$ was considered statistically significant.

RESULTS

Speed of Sound Through Normal Pulmonary Components

Two-dimensional color-coded images from specific areas (2.4×2.4 mm) were obtained within a few minutes of each scanning (Figure 1). Pulmonary structures such as alveoli, bronchial trees, blood vessels, and stromal connective tissues were recognized corresponding to those visualized using a light microscope (Figure 2a–e).

The speed of sound through each pulmonary tissue element are compared in Table 1 and Figure 2f. The speed through normal alveoli, bronchial walls, congested alveoli, fibrosis with organizing pneumonia, cartilage, vascular smooth muscles, and blood increased gradually in this order. The mean speed through each component was significantly different from that through normal alveoli ($P < 0.01$).

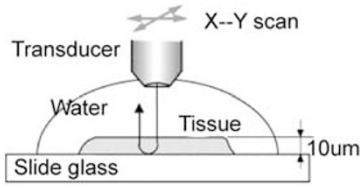

Figure 1 Scanning acoustic microscope. The ultrasound emitted by an acoustic transducer hits or penetrates the tissue and is reflected onto the surface of the tissue or glass slide. It is then returned to the detector. The speed of sound through the tissue is calculated by comparing the 'time of flight' of the pulse from the surfaces of both tissue and glass.

Detection of Focal Abnormal Lesions by SAM

Focal lesions in the lung such as pulmonary congestion, pneumonia with fibrosis, hemorrhagic edema, and senile emphysema (Figure 3a and b) were well visualized and comparable to those visualized using the light microscope. Compared with surrounding tissues, areas of hemorrhage, fibrosis, and muscle fibers corresponded to areas with greater sound speed.

About lymph nodes in the lung, carcinoma with desmoplastic reaction were detected by SAM (Figure 3c). The speed of sound was greater through the metastatic site than through lymphoid tissue.

Neoplasms with Hypervascularity or Desmoplastic Reactions Show Increased Speed of Sound

Lung ADCs develop from *in situ* BACs. Desmoplastic ADC reactions discriminate BACs. BACs grow along alveolar walls and are occasionally missed diagnostically because the histology mimics that of normal alveolar structures. Stromal hypervascularity of BACs discriminate normal alveoli. SAM distinguished BACs from normal alveoli and invasive ADCs from BACs. Figure 4a and b shows characteristic images that discriminate between these lesions, and statistical analysis also demonstrated significant differences (Figure 4c).

Idiopathic interstitial pneumonia is characterized by particular histological types. UIP presents the worst prognosis, with NSIP having a significantly better prognosis. Fibrosis was patchy and denser in UIP compared with its uniform and looser appearance in NSIP. Acoustic images obtained using SAM could discriminate between these two lesions (Figure 5a and b). Statistical analysis also confirmed the difference in speed of sound between the two lesions (Figure 5c).

Discrimination of Amyloid Deposition Disease by SAM

In systemic amyloidosis, amyloid fibrils deposit along vascular walls. Although Congo red staining visually confirmed

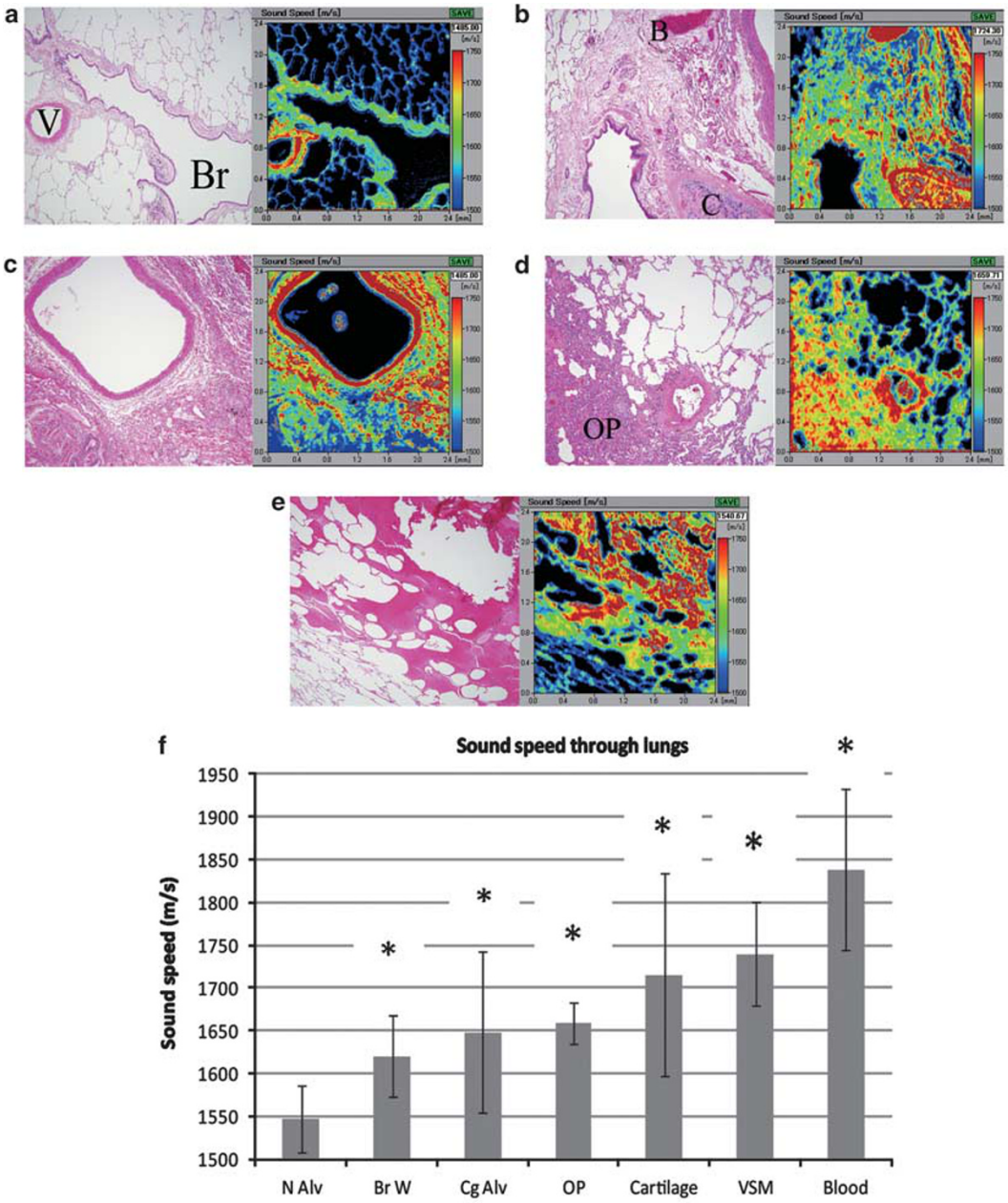

Figure 2 (**a**) Normal lung consisting of bronchioles (Br), alveoli, and blood vessels (V). The light microscopic (LM) image (left) with hematoxylin and eosin (HE) staining and its corresponding acoustic image (right). The speed of sound was lesser through alveoli than through bronchial walls and vascular smooth muscle. (**b**) Normal lung bronchovascular bundle consisting of connective tissues. The LM image (left) with HE staining and its corresponding acoustic image (right). The speed of sound was greater through the peribronchial fibrous connective tissue than through alveoli. The speed was greatest through bronchial cartilage (C) and intravascular blood (B) (>1700 m/s). (**c**) Congested lung with dilated pulmonary vein and blood-filled alveoli. The LM image with HE staining (left) and its corresponding acoustic image (right). The speed of sound was greater through vascular smooth muscle and blood-filled alveoli than through normal alveoli. (**d**) Areas of fibrosis with organizing pneumonia (OP). The LM image with HE staining (left) and its corresponding acoustic image (right). Areas of fibrosis with organizing pneumonia showed greater sound speed than surrounding alveoli. (**e**) Focal pulmonary hemorrhage. The LM image with HE staining (left) and its corresponding acoustic image (right). An area of hemorrhage showed greater sound speed than normal alveoli. (**f**) The speed of sound through pulmonary structures. Mean sound speed (m/s) and s.d. are shown. *$P<0.01$ *versus* normal alveoli.
Br W, bronchial wall; Cg Alv, congestive alveoli; N Alv, normal alveoli; OP, organizing pneumonia; VSM, vascular smooth muscle.

pulmonary amyloid deposits, these were occasionally missed because of weak staining. Acoustic imaging using SAM apparently detected abnormally greater sound speed at deposition sites (Figure 6a). Statistical analysis also confirmed a significant difference between the amyloid deposition area and normal alveolar walls (Figure 6b).

Table 1 The speed of sound (mean ± standard deviation) through pulmonary structures

Structure	*n*	Mean	Standard deviation
N Alv	468	1547	40
Br W	152	1621	47.9
Cg Alv	25	1648	94.1
OP	37	1659	24.9
Cartilage	19	1715	118.4
VSM	136	1740	61.1
Blood	16	1839	93.5
BAC	185	1598	30.5
ADC	34	1634	36.7
UIP	428	1618	55.3
NSIP	204	1572	47.8
Amyloid	105	1617	51

Abbreviations: ADC, adenocarcinoma; BAC, bronchioloalveolar carcinoma; Br W, bronchial wall; Cg Alv, congestive alveoli; N Alv, normal alveoli; NSIP, non-specific interstitial pneumonia; OP, organizing pneumonia; UIP, usual interstitial pneumonia; VSM, vascular smooth muscle.

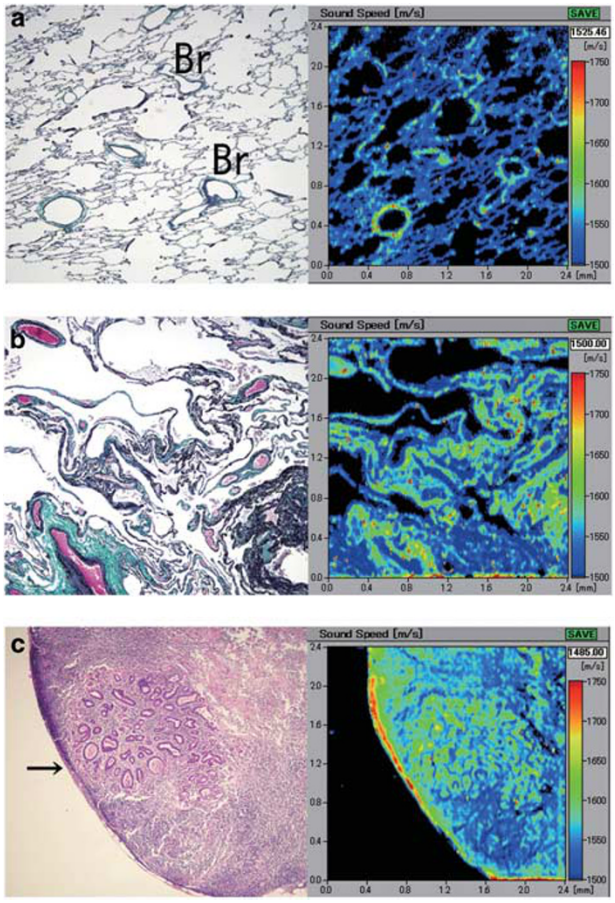

Figure 3 (**a**) Pulmonary emphysema in a young patient. The light microscopic (LM) image with Elastica–Masson staining (left) and its corresponding acoustic image (right). Some air spaces are dilated although the alveolar structure is well preserved with homogeneously thin walls. The speed of sound through alveolar walls was similar to that through normal alveoli. Br, bronchioles. (**b**) Pulmonary emphysema in an elderly patient. The LM image with Elastica–Masson staining (left) and its corresponding acoustic image (right). The speed of sound through emphysema with dilated air spaces was almost identical to that through bronchial walls. Normal alveolar structures had almost disappeared in this section. (**c**) Metastatic adenocarcinoma in a lymph node. The LM image with hematoxylin and eosin (HE) staining (left) and its corresponding acoustic image (right). Gastric adenocarcinoma forms nest in the marginal sinus with stromal desmoplastic reaction (arrow). The speed of sound through the metastatic site shows greater sound speed than surrounding lymphoid tissue.

DISCUSSION

The concept of the acoustic microscope was first suggested in 1936 by SY Sokolov, but the technology for generating high-frequency sound and processing the signals thus generated became available only in the 1960s.[6] The first practical SAM was developed in 1974 by Lemons and Quate.[7] Many improvements to the system have since been made to enhance accuracy. Ultrasonic imaging is generally performed with sound at frequencies ranging from 2 to 15 MHz, but SAMs operate at frequencies ranging from 100 MHz to 3 GHz because of the requirement for high resolution. At 3 GHz, the acoustic wavelength in water is 520 nm, which corresponds to the optical wavelength of green light.[6]

Correlation between the composition of a tissue and its acoustic properties is the most important issue to be addressed in tissue studies. Mechanical properties on the tissue level are controlled by water content, connective tissue properties, pressure in blood vessels and interstitial liquid, peculiarities in intercellular material, and aggregation and interaction of cells.[8]

As a rule, sound speed increases according to the hardness of the tissue, which is often dependent on collagen/muscle fibers or cell density. Color-coded lung images obtained using SAM corresponded well with LM images. The mean speed through each component or lesion varies significantly, enabling accurate statistical analysis among lesions.

Differential diagnosis between UIP and NSIP is sometimes difficult histologically. However, using SAM, we could calculate the speed of sound through fibrous lesions and predict the possible histological type involved. The sound speed was significantly greater for UIP than for NSIP.

Discrimination of BACs from normal alveoli is sometimes difficult because clinging spread of BACs mimics normal alveolar structures. Hypervascularity resulting due to the nutritional requirement of neoplasm increases the thickness of alveolar walls. SAM is well suited to detect this hypervascularity and can detect the difference in sound speed between BAC and normal alveolar walls.

Invasive ADCs present a worse prognosis than *in situ* BACs. The level of desmoplastic reactions depends on the extent of tumor invasion, and because sound speed increases

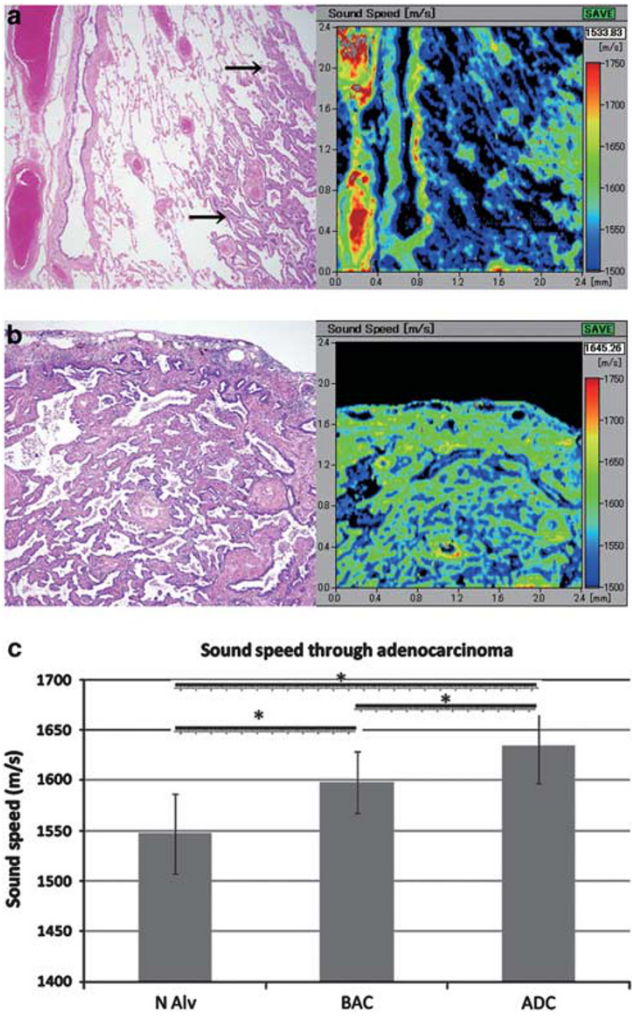

Figure 4 (**a**) Bronchioloalveolar carcinoma (BAC) replacing alveolar walls. The light microscopic (LM) image with hematoxylin and eosin (HE) staining (left) and its corresponding acoustic image (right). BAC or adenocarcinoma (ADC) *in situ* is adherent to the alveolar walls on the right side (arrows). The alveolar walls are thicker than normal alveoli and showed greater sound speed, identical to that showed by bronchial walls. (**b**) Partially invasive lung ADC with BAC-like spread. The LM image with HE staining (left) and its corresponding acoustic image (right). Invasive ADC in the pleura (upper) showing desmoplastic reactions, which correspond to areas of greater sound speed. BAC-like spread seen in the parenchyma exhibits trabecular structures, with sound speed similar to that of the desmoplastic pleural area. (**c**) The speed of sound through normal alveoli (N Alv), BAC, and ADC. N Alv, 1547 ± 40.0 m/s (mean ± s.d.), $n = 468$; BAC, 1598 ± 30.5 m/s, $n = 185$; ADC, 1634 ± 36.7 m/s, $n = 34$; $^*P < 0.01$.

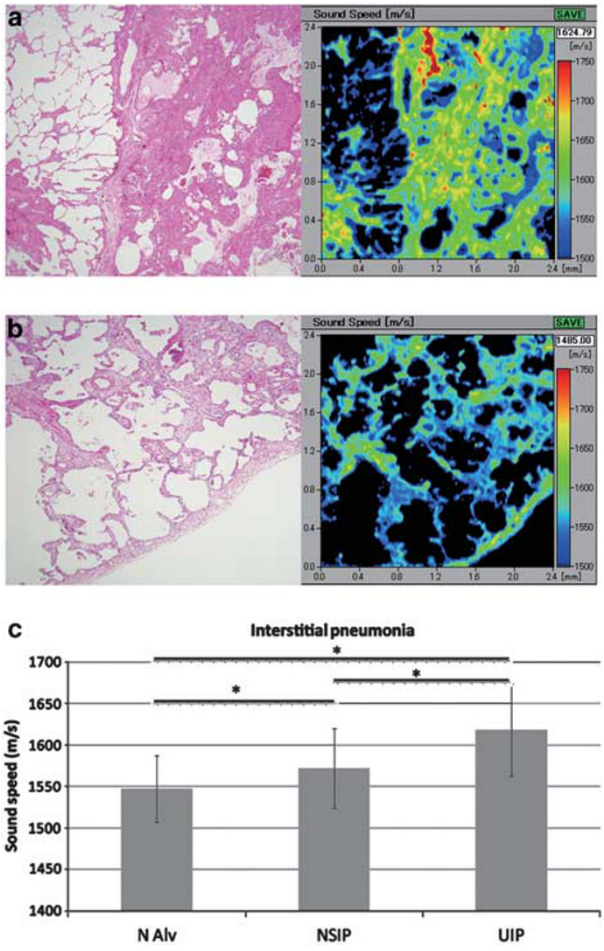

Figure 5 (**a**) Usual interstitial pneumonia (UIP). The light microscopic (LM) image with hematoxylin and eosin (HE) staining (left) and its corresponding acoustic image (right). The thick fibrotic area (right) showed greater sound speed than normal alveolar areas (left). The denser fibrous areas showed greater sound speed. (**b**) Non-specific interstitial pneumonia (NSIP). The LM image with HE staining (left) and its corresponding acoustic image (right). Fibrous septa surrounding the air spaces showed greater sound speed than normal alveoli. Cellular areas with lymphocytic infiltration showed lesser sound speed than fibrotic areas. (**c**) The speed of sound through normal alveoli (N Alv), NSIP, and UIP. N Alv, 1547 ± 40.0 m/s (mean ± s.d.), $n = 468$; NSIP, 1572 ± 47.8 m/s, $n = 204$; UIP, 1618 ± 55.3 m/s, $n = 428$; $^*P < 0.01$.

in accordance with fibrosis, acoustic images using SAM can predict the extent of tumor invasion.

Both metastatic and inflammatory lymph nodes enlarge. Hardness is a good indicator of differentiation of cancer metastasis, and SAM is applicable in this situation. Images obtained using SAM reflected distinct metastatic cancers in lymph nodes[9] as shown in Figure 3c.

Organs with amyloid deposits usually show rigidity with hemorrhagic tendency. In our observations using SAM, amyloid deposition areas in all organs demonstrated greater sound speed than surrounding tissues.[9]

SAM provides three major benefits. First, it needs no special staining and takes only a few minutes to acquire images. Second, it provides basic data for low-frequency ultrasonic examination, including ultrasonic endoscopy[10] for organs such as the GI tract and bronchus, and elastography of organs such as the breast[11] and liver.[12] Third, sound speed data from each point are digital, so that statistical analysis is easy to compare between lesions or diseases.

Although fresh frozen tissue is better than formalin-fixed, paraffin-embedded tissue for evaluation of natural acoustic properties, frozen sections need special techniques to prepare

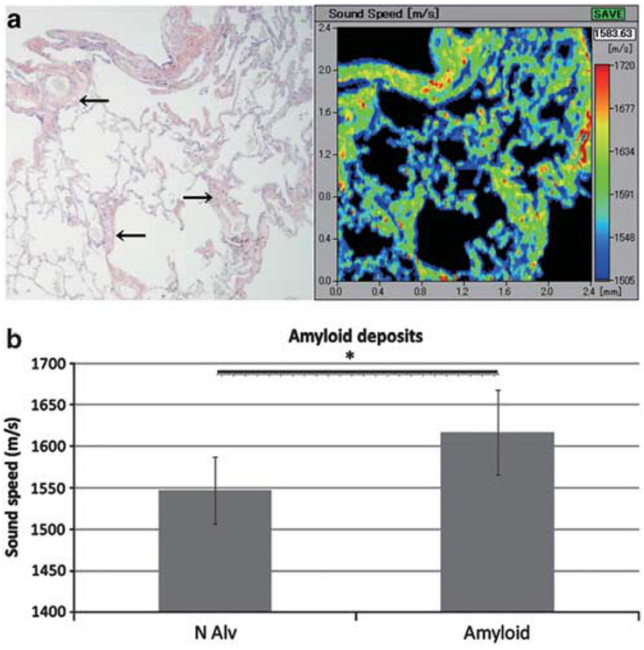

Figure 6 (**a**) Lung amyloidosis. The light microscopic (LM) image with Congo red staining (left) and its corresponding acoustic image (right). An amyloid deposit is stained red in perivascular areas (arrows), which reveal thicker vascular walls with greater sound speed than normal alveolar walls. (**b**) The speed of sound through normal alveoli (N Alv) and amyloid deposits on alveolar walls. N Alv, 1547 ± 40.0 m/s (mean ± s.d.), $n = 468$; amyloid deposits, 1602 ± 51.0 m/s, $n = 105$; $^*P < 0.01$.

uniformly flat sections. Sasaki *et al*[13] reported that no significantly variable properties of the normal kidney were found between these different preparations. Our preliminary data on lung tissues also showed no significant difference in sound speed between formalin-fixed and fresh frozen tissues.

Supplementary Information accompanies the paper on the Laboratory Investigation website (http://www.laboratoryinvestigation.org)

ACKNOWLEDGEMENTS

We thank Dr K Kobayashi (Honda Electronics Co., Ltd., Toyohashi, Japan) for his technical supports and advices with SAM, and S Okamoto, T Kato, Y Kawabata, and N Suzuki for preparing the tissue sections. This work was supported in part by grants from the Japan Science and Technology Agency (AS232Z01789F), the Ministry of Education, Culture, Sports, Science and Technology of Japan (24590445). We would also like to thank Enago (www.enago.jp) for the English language review.

DISCLOSURE/CONFLICT OF INTEREST

The authors declare no conflict of interest.

1. Wells PNT. Velocity Absorption and Attenuation in Biological Materials in Biomedical Ultrasonics, London, 1977) pp110–137.
2. Saijo Y, Saijo Y, Tanaka M, *et al.* Ultrasonic tissue characterization of infarcted myocardium by scanning acoustic microscopy. Ultrasound Med Biol 1997;23:77–85.
3. Sasaki H, Sasaki H, Saijo Y, *et al.* Characterization of renal angiomyolipoma by scanning acoustic microscopy. J Pathol 1997;18: 455–461.
4. Hozumi N, Yamashita R, Lee CK, *et al.* Time-frequency analysis for pulse driven ultrasonic microscopy for biological tissue characterization. Ultrasonics 2004;42:717–722.
5. Kijima H, Minagawa H, Saijo Y, *et al.* Degenerated coracoacromial ligament in shoulders with rotator cuff tears shows higher elastic modulus: measurement with scanning acoustic microscopy. J Orthop Sci 2009;14:62–67.
6. Maugh II TH. Acoustic microscopy: a new window to the world of the small. Science 1978;201:1110–1114.
7. Lemons RA, Quate CF. Acoustic microscopy: biomedical applications. Science 1975;188:905–911.
8. Maev RG. Application of acoustic microscopy methods in studies of biological objects. In: Acoustic Microscopy Fundamentals and Application, Weinheim, Germany, 2008, pp187–190.
9. Miura K, Yamamoto S, Kobayashi K. Clinical application of ultrasonic microscopy UM; for histological examination. J FASEB 2011;25:6811.
10. Ernst A, Feller-Kopman D, Herth FJ. Endobronchial ultrasound in the diagnosis and staging of lung cancer and other thoracic tumors. Semin Thorac Cardiovasc Surg 2007;19:201–205.
11. Itoh A, Ueno E, Tohno E, *et al.* Breast disease: clinical application of US elastography for diagnosis. Radiology 2006;239:341–350.
12. Rockey DC. Noninvasive assessment of liver fibrosis and portal hypertension with transient elastography. Gastroenterology 2008;134: 8–14.
13. Sasaki H, Saijo Y, Tanaka M, *et al.* Influence of tissue preparation on the high-frequency acoustic properties of normal kidney tissue. Ultrasound Med Biol 1996;22:1261–1265.